99-213

Environment Canada / Environnement Canada

Canada

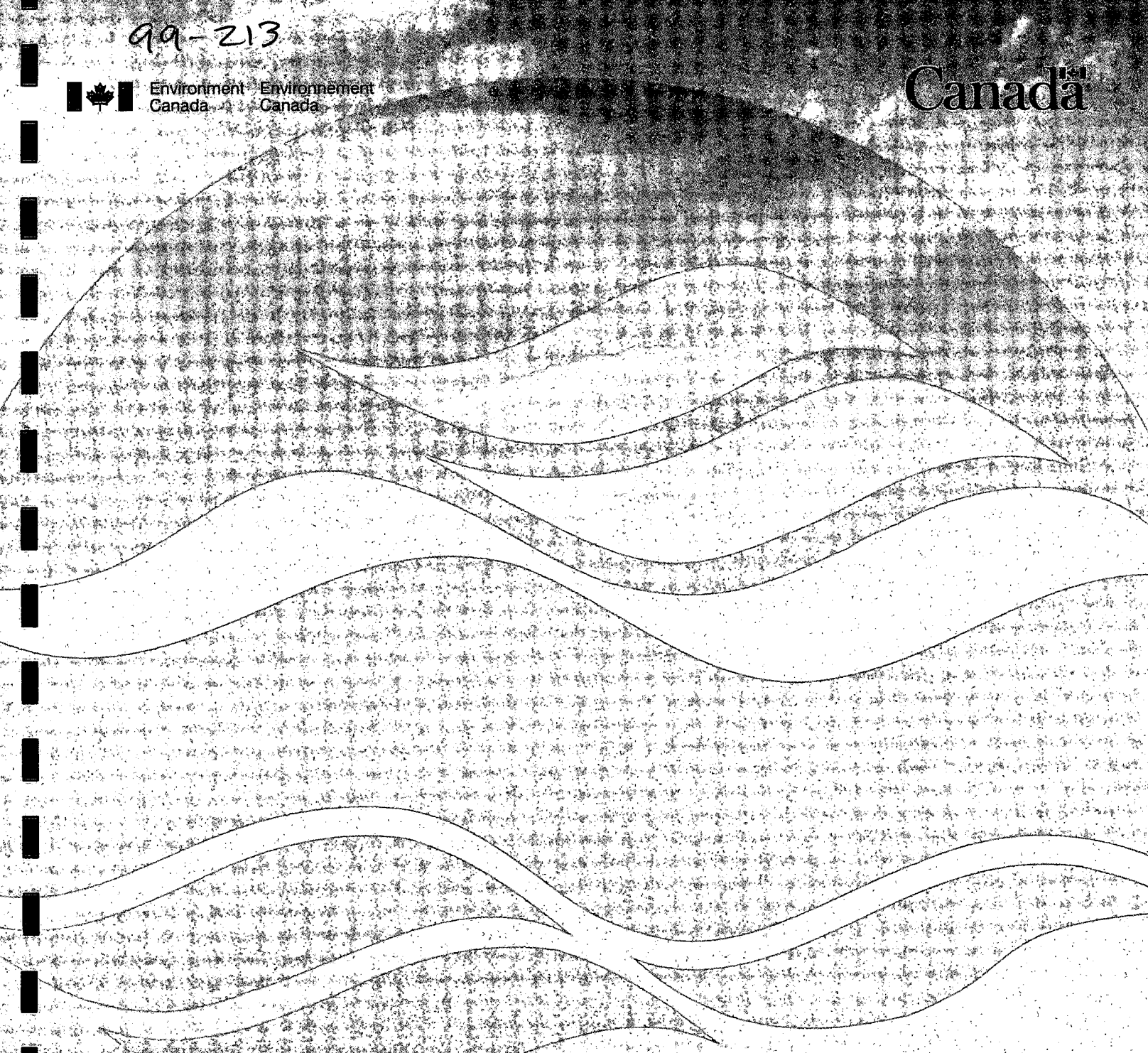

Capturing More Geological Realism In Stochastic Simulations of Rock systems with Markov Statistics and Simulated Annealing

BY:

K. Parks, L. Bentley, A. S. Crowe

NWRI contribution No. 99-213

CAPTURING MORE GEOLOGICAL REALISM IN STOCHASTIC SIMULATIONS OF ROCK SYSTEMS WITH MARKOV STATISTICS AND SIMULATED ANNEALING

Kevin Parks[1]
Laurence R. Bentley[2]
Allan S. Crowe[3]

1: Petro-Canada Oil and Gas Ltd., P.O. Box 2844, Calgary, Alberta, T3P 3E3
2: Department of Geology and Geophysics, University of Calgary, Calgary, Alberta, T2N 1N4
3: National Water Research Institute, Canada Centre for Inland Waters, P.O. Box 5050, Burlington, Ontario, L7R 4A6

submitted to Journal of Sedimentary Research, Part B.

February, 1999

MANAGEMENT PERSPECTIVE

The environmental and human health threats posed by toxic substances and other substances of concern are prevented or reduced.

Environment Canada needs reliable information to assess and predict the fate and transport of contaminants in the groundwater environment. The numerical model discussed in this paper is designed to simulate bedding relationships in outwash deposits. This model can be used to estimate hydrogeological properties of these sediments, and hence provide important information for the prediction of the transport and fate of contaminants in a groundwater environment. The project originally designed to assist in understanding of the hydrogeological environment at the Gloucester Landfill toxic waste site, Ottawa. It also has wider implications for the control of contaminant loadings through cyclic sediments to coastal wetlands in the Great Lakes basin.

This paper resulted from a collaborative research program with Dr. L. Bentley, Dept. of Geology and Geophysics at the University of Calgary is continuing during FY 96/97. Ph.D. student, K. Parks, developed the numerical model as part of his Ph.D. thesis. During FY 98/99, the graduate student completed his thesis, defended, and this paper is a direct product of the thesis .

Nothing further is planned at this time.

SOMMAIRE À L'INTENTION DE LA DIRECTION

On prévient ou on réduit les risques pour l'environnement et pour la santé humaine posé par les substances toxiques et par d'autres substances préoccupantes.

Environnement Canada a besoin d'informations fiables pour évaluer et prévoir le devenir et le transport des contaminants dans les eaux souterraines. Le modèle numérique examiné dans cette publication doit simuler les rapports de litage dans les dépôts d'épandage fluvio-glaciaire. On peut utiliser ce modèle pour évaluer les propriétés hydrogéologiques de ces sédiments et obtenir ainsi des informations importantes pour la prévision du transport et du devenir des contaminants dans les eaux souterraines. On a d'abord conçu ce projet pour faciliter la compréhension du milieu hydrogéologique de la décharge de déchets toxiques de Gloucester (Ottawa). Ce modèle présente également un intérêt plus général pour la limitation des charges de contaminants par des sédiments cycliques aux lieux humides côtiers dans le bassin des Grands Lacs.

Cette publication est le résultat d'un programme de recherches effectuées en collaboration avec M. L. Bentley, du Département de géologie et de géophysique de l'Université de Calgary, qui s'est poursuivi au cours de l'AF 1996/97. Un étudiant du troisième cycle, M. K. Parks, a développé le modèle numérique dans le cadre de sa thèse de doctorat. Au cours de l'AF 1998/99, il a terminé la rédaction de sa thèse et l'a défendue, et cette publication est basée directement sur cette dernière.

On ne prévoit aucune autre activité pour l'instant.

RÉSUMÉ

On peut utiliser la méthode du recuit simulé pour superposer des structures statistiques markoviennes à des champs aléatoires structurés représentant l'hétérogénéité rocheuse. Cette approche permet d'utiliser des conditions plus réalistes du point de vue géologique dans les simulations stochastiques destinées aux simulateurs d'écoulement. Les matrices de probabilité de transition de Markov sont encodées dans des histogrammes multipoints à l'intérieur d'une fonction objective, et on construit ensuite des champs catégoriques 2D par recuit simulé. Les questions de rendement nuisant à l'utilisation du recuit simulé avec les fonctions objectives markoviennes sont notamment les distributions catégoriques des échelles de longueur, les importances relatives des échelles de longueur par rapport à la taille de la grille et la complexité des structures de Markov intercalées. Pour y remédier, il est recommandé, notamment, de sélectionner une taille de grille appropriée, de choisir avec soin le type de recuit et de tenir compte d'autres critères basés sur le test statistique du chi carré, souvent utilisé dans les analyses markoviennes. À l'aide de structures de Markov, on peut alors faire appel à des structures réalistes sur le plan géologique comme la dépendance à l'égard d'éléments d'ordre supérieur, la cyclicité et la directionalité. On peut utiliser le rééchelonnement temporel pour assurer un transfert à l'horizontale adéquat de structures markoviennes verticales dans le cadre d'une adaptation probabiliste de la loi de Walther. Cette technique est démontrée par des exemples hypothétiques et observés sur le terrain.

ABSTRACT

Simulated annealing can be employed to impose Markovian statistical structures on structured random fields representing rock heterogeneity. By this approach one can transmit more geological realism into stochastic simulations for flow simulators. Markov transition probability matrices are encoded into multi-point histograms within an objective function and then 2D categorical fields are constructed with simulated annealing. Peformance issues that compromise annealing with Markovian objective functions include categorical length-scale distributions, relative magnitudes of length scales to grid size, and complexity in embedded Markov structures. The remedies to these issues include proper selection of grid size, careful choice of type of annealing and consideration of alternative stopping criterion based on a chi-squared test statistic common in Markovian analysis. Geologically realistic structures like higher order dependency, cyclicty, and directionality can be enforced by employing Markov structures. Temporal rescaling can be used to ensure proper transferrence of vertical Markovian structures to the horizontal under a probabilistic restatement of Walther's Law. Hypothetical and field examples demonstrate the technique

INTRODUCTION

Stochastic simulation of heterogenous rock for flow simulators can be done by a variety of methods (e.g., Koltermann and Gorelick 1996). A practical challenge to their implementation remains how to better constrain simulations to match geological concepts of reasonableness (Deutsch and Hewitt 1996). In the parlance of stochastic simulations, constraining outputs through conditioning with prior knowledge reduces the space of uncertainty explored by the outcomes and thus increases their utility in decison-making.

Doveton (1994) suggests that Markov models can play a role in transmitting more geological realism into simulator grids. Markov statistics encapsulate information on relationships between categories as well as length-scale information. In their common form, Markov statistics are presented in form of a transition probability matrix. The matrix tabulates the probability that a time or space series stays in the same state or enters a different state with each succeeding step. Davis (1986) provides a complete introduction.

Markov structures have long been used by geologists to identify and quantify facies and stratigraphic relationships in bedding sequences (e.g., Schwarzacher 1975; Walker 1979; Xu and MacCarthy 1996). Various methods exist to directly generate Markov fields (Krumbein 1967; Harbaugh and Bonham-Carter 1970; Lin and Harbaugh 1984; Moss 1990; Luo 1996) or use Markov structures to improve, inform, or calibrate other geostatistical or geosystem simulation methods (e.g., Murray 1994; Carle and Fogg 1996). Despite their obvious attraction to geologists, Markov fields have had relatively little penetration into the practice of stochastic simulation. Koltermann and Gorelick (1996) cite the difficulty of conditioning pure Markov fields to other types of field data as a barrier to their practical use. Whereas pure Makov fields may have limited applicability in stochastic reservoir simulation, we propose that the enforcement of Markov structures in stochastic fields is still worthy of pursuit because they are amenable to the capture and expression of some geologically meaningful attributes of stratal architecture.

In this paper we document the construction of two-dimensional stochastic fields with Markov properties by simulated annealing using the multipoint histogram method of Deutsch and Journel (1992). We demonstrate how annealing performance is affected if Markov structures are being enforced. As well, we demonstrate that meaningful stratal geometries can be effectively reproduced in stochastic fields by imbuing them with a Markov structure. We underscore that conventional geologic reasoning offers ample justification for building multidimensional random fields with Markov properties from observations of vertical bedding.

CONSTRUCTING MARKOV FIELDS WITH SIMULATED ANNEALING

Markov Chains and Fields

A sequence of events wherein the present state of the sequence is contingent on the state of the sequence at some time prior to the present is said to be a Markov chain. The structure of a Markov chain can be summarized in a "transition frequency matrix", wherein the frequencies of transition from any one state to itself or the other states are tabulated (in columns) by state (the

rows). If the frequencies are normalized by the row totals, the matrix provides the probability of transition from any state to any other in a unit step. A chi-squared test is usually applied to an experimental Markov matrix to determine if the transitions collectively or individually are significantly different than a random series of events (Davis, 1986). Two and three dimensional spatial fields can also have Markov properties (Lin and Harbaugh 1984). Detailed discussion of the relationships between stratal patterns and Markov structures are found in Harbaugh and Bonham-Carter (1970) and Schwarzacher (1975) as well as the references cited above.

Simulated Annealing

Simulated annealing is a global optimization method whereby a field that honors an idealized set of control statistics can be generated in a stochastic framework. Gateway references to the details of annealing methodology are Ouenes and Bhagavan (1994) and Jensen et al.(1997). The essence of the annealing methodology is summarized below.

To generate a stochastic field or image by annealing, an ideal or training field is first characterized by a combination of statistical or other descriptive measurements. A trial field is then generated. The trial field can be a totally random image matching the ideal global histogram or a structured field created by a different algorithm. The same descriptors are calculated for the trial field. An objective function, O, is then computed as the difference or squared difference between the ideal and trial field descriptors. The components of the objective function may be weighted to assign equal importance to small and large values or components with different units of measurement. The trial field is then perturbed, usually by replacing the value of one of the field elements with another drawn from the underlying global histogram or by swapping two nodes at random. The objective function is recalculated. Perturbations that reduce the value of the objective function are kept. Perturbations that increase the value of the objective function are accepted with a probability that decreases in proportion to the increase in objective function scaled by a parameter called the "temperature". If the values of O are normalized by the original value, then the formal probability rule for acceptance (eqn. 1) is a Boltzman distribution of the form:

$$P_{accept} = exp(\frac{O_{old} - O_{new}}{T}) \qquad \text{(Equation 1)}$$

where P_{accept} is the probability of accepting a perturbation, O_{old} is the normalized value of the objective function calculated before the perturbation, O_{new} is the normalized value of the objective value calculated after the perturbation, and T is the temperature, initially set to 1 (Jensen et al. 1997)

If a pre-chosen number of perturbations are accepted (usually of the order of 10N where N is the number of elements in a field) before some maximum number of total perturbations (of the order 100N), the temperature is reduced by some factor less than 1 (usually 0.1). Fast updating schemes are employed to avoid completely recalculating O after every perturbation, for instance only subtracting the contribution of the perturbed field values from O and then adding contribution of the new values (e.g., Deutsch and Journel 1992). This procedure is repeated until the objective function falls below a threshold or its value can no longer be reduced. A very low value of O, of the order $1x10^{-6}$, means that the annealed field closely matches the desired attributes encoded in the objective function.

The change in the value of O with perturbations is called the objective function trajectory. The standard implementation of annealing employing Equation 1 allows hill-climbing to avoid undesirable local minima along the objective function trajectory. Steepest-descent or iterative improvement variants, where only improvements are accepted, can also used. These variants are much faster but can be prone to becoming trapped in local minima, depending on the nature of O.

Formulation of the Objective Function for Constructing Markov Fields

A Markov transition matrix can be easily encoded in an annealing objective function as a series of multipoint histograms as first described by Farmer (1992). Two-point histograms denote the expected number of transitions from any state i to any state j for a given lag in a given direction. For the forward direction of a simple Markov chain, the expected number of transitions f, between states i and j in an nx•ny•nz field that uses edge-wrapping to avoid edge effects (Deutsch and Cockerham 1994) is:

$$f_{ij} = P(i) \bullet P(j|i) \bullet nx \bullet ny \bullet nz \qquad \text{(Equation 2)}$$

where P(i) is the proportion of state i and P(j|i) is the probability of transition to state j given that you are in state i. The proportion of state i can be found by powering the transtion matrix until the columns values stabilize. More complex Markov structures can be built using multiple dependencies and encoded in a similar fashion. Markov chains wherein the state at any point depends upon the state at more than one location or time prior to that point are said to have a higher order structure. For example, if the state depends upon the state at a time or location immediately prior as well as the state two lags prior, we say the chain is a second-order Markov structure. Higher order structures in geologic materials suggest the presence of multiple, independent processes acting at different scales in the deposition process.

In our implementation, the following objective function is enforced to generate two-dimensional, first-order fields:

$$O = \frac{1}{O^o}\{\sum_{idir=1}^{2} \sum_{i=1}^{im} \sum_{j=1}^{im} [\frac{[f_{idir,i,j}^{train} - f_{idir,i,j}^{real}]^2}{f_{idir,i,j}^{train}}] \qquad \text{(Equation 3)}$$

where O is the value of the nomralized objective function, i and j are state indices, im is the number of states, $f_{idir,i,j}^{train}$ is the number of transitions from i to j in the idirth direction of the ideal or training image, and $f_{idir,i,j}^{real}$ is that value calculated for the current image being annealed . The calculated value of the objective function is normalized by the initial non-normalized value of O, O^o. The squared difference between $f_{idir,i,j}^{train}$ and $f_{idir,i,j}^{real}$ is divided by $f_{idir,i,j}^{real}$ to give more equal weighting to small values of transition frequencies.

Performance Issues

The main appeals to continued research in the applications of simulated annealing are: 1) its lack of an underlying statistical model, 2) its ability to condition stochastic fields with information

from disparate sources, and 3) the hope that future improvement in computer performance will eventually reduce the computional expense to levels comparable to presently faster algorithms. If Markov structures are to be enforced in stochastic fields through simulated annealing, then the following performance issues need to be considered:

- Scale Effects
- Complexity Effects
- Implementation Strategy
- Stopping Criteria
- Effect of Conditioning.

The impact of these issues on annealing of fields with Markov structures are illustrated by examples in this section using both hypothetical and field-data derived Markov structures.

Table 1 shows four hypothetical, 3-state, first-order Markov transition matrices that are used in the examples. The length scale of any one state in a Markov chain can be described by any number of measures. The thickness or duration of a state in a first-order Markov process will be geometrically distributed with an arithmetic mean approximated by (Doveton 1994):

$$p_{ii} = \frac{p_{ii}}{1-p_{ii}}\Delta \qquad \text{(Equation 4)}$$

where p_{ii} is the value of the diagonal element in the ith row of transition probabilty matrix and Δ is the step length in the chain. In the transition probability matrices 1A and 1B, all the values along the diagonal are identical, implying that there are no differences in the average length-scales of the bodies of each state. In Tables 1C and 1D, the values along the diagonals are different, implying that the average length scales are different between the three states.

The transitions between different states in a Markov chain are encapsulated in the embedded form of the transition proability matrix, also shown in Table 1. The embedded form is calculated by setting the diagonal values to zero and renomalizing the off-diagonal elements by their sum. In

the embedded form of 1A, there is no preferred transition from any state to any other, meaning that the juxtoposition of the bodies has no structure. In the embedded form of Table 1B, there is a preferred pattern of state-to-state transitions B-G-W-B-G-W..., since there is three times the probabilty of going to state G from B than W and so on. This repetition is referred to as cyclicity. If there is asymmetry in the cyclicity if the chain direction was to be reversed, the Markov chain is said to possess the property of directionalty. The chain in Table 1B shows directionality. The embedded form of matrix 1C is the same as 1B. The embedded form of 1D has more of a random component because there is no preference from state W to either B or G.

For comparison, a first-order, five-state Markov chain derived from real field data is shown in Table 2. The lithologic data in the transition frequency matrix come from vertical cores taken from boreholes through a finely interbedded, glaciolacustrine sedimentary sequence at the Gloucester landfill site near Ottawa, Ontario. The sediments are interpreted to be deposits of coalescent, subaqueous deltas that built out from subglacial drainage tunnels into meltwater lakes in front of retreating glaciers. At this site, this layer acts as an aquitard or confining layer, hydraulically separating a surficial aquifer from a deeper, saturated glacio-fluival sand aquifer which hosts a contaminated groundwater plume (Jackson et al. 1991; Gailey and Gorelick 1995).

The lithologies were logged at regular intervals within each of the cores. The number of transitions from any state to iteslf or different states along a single 2-mm step were then counted to form the transition matrix.The results from all the boreholes were then combined under the assumptions that the process of formation was homogenous across the drill-site and that the boreholes were far enough from each other to represent independent samples of the process of deposition. In this case, a chi-squared test determined that the Markov matrix as a whole was significantly different than a random series of events, mainly because the sediments are layered at about a 10 to 50-cm scale and the transition frequency matrix is overwhelmingly diagonally dominant. No significant higher order structure could be detected. The embedded Markov structure was determined to be no different than a random series of events, which is consistent to the interpretation that the sedimentary process was dominated by episodic events linked to ice-wasting. Detailed analysis however did indicate a significant association of diamict and overlying medium sand, suggesting a linked origin in the depositional system. In the final analysis,

however, the random signal associated with episodic events presumably triggered by glacial wasting is thought to have overwhelmed the more regular, autocyclic, prodelta sedimentary processes predicted by a simper sedimentological model of delta processes (Parks 1998).

Effect of Length Scale

Annealing fields with Markov properties on finite grids becomes increasingly difficult as the length-scale of the bodies become large relative to the size of the grid. Figure 1 shows the objective function trajectories for annealing single realizations of 3-state, first-order structure with no embedded structure. The trajectory A corresponds to the transition probability matrix in Table 1A where the diagonal elements are 0.60. The transition probability structure was imposed isotropically in both the x and y directions on a regular 100x100 unit field. The other trajectories on Figure 1 represent the same matrix but where the diagonal elements have been increased to 0.70, 0.80, and 0.90. The mean body length in the x and y directions are increasing relative to the dimension of the field (Eqn. 4). As the mean body length increases relative to the field size, more perturbations are required to reduce the normalized objective function to an acceptable minimum value (in this case $1x10^{-6}$). In the last case, where p_{ii}=0.90, the ratio of grid dimension to body length is nearly 10 and the maximum number of perturbations at one temperature is exceeded before the stopping criterion is reached.

Effects of Increasing Complexity

Annealing performance deteriorates as the Markov structure becomes increasingly complex in terms of numbers of states, the complexity in the embedded form, and difference in length-scale distributions between states. Figure 2 shows the five objective function trajectories for single, 100x100 unit realizations created from Table 1A through 1D and Table 2. Iterative improvement was used. From the discussion above, we can see that of the five structures presented, Table 1A has the least structure - bodies of identical length-scale distributions and no embedded structure. Table 1B has bodies of identical length-scales but cyclicity and directionality in the embedded structure. Table 1C has different length-scale distributions plus cyclicity and directionality whereas 1D has more randomness than 1C. Table 2 has a greater degree of randomness in its

embedded form as well as has five states with different length scale-distributions. The combined effect of increasing complexity and increasing length-scales relative to grid size increase the number of perturbations needed to successfully anneal the field. In the case of the Gloucester structure, the slope of the objective function trajectory was too shallow to reach the desired minimum value of O in an acceptable number of perturbations.

Implementation Strategy

As documented in the references above, there are a number of variants of annealing that can be employed to create stochastic fields. To anneal our Markov fields, we employed a strategy whereby the random fields were seeded with the expected proportions of each state determined by powering the transition probability matrix. Perturbations were done by swapping pairs of grid values selected at random. In general, iterative improvement performed acceptably well with 3-state, first-order Markov structures. As length-scales, number of states, complicated embedded structures etc. were incorporated, true annealing with "hill-climbing" tends to perform better. In the case generating a 100x100 field for the 5-state Gloucester transition structure, neither true annealing or iterative improvement were sufficient on their own to reduce the normalized objective function below an acceptable threshold in an acceptable number of perturbations. The objective function trajectories for two attempts are shown in Figure 3. In the case of pure iterative improvement, the objective function trajectory becomes trapped in an unacceptable local minimum. In the case of pure annealing alone, the objective function trajectory does not descend quickly enough to reach the desired threshold in less than $2x10^7$ perturbations. Post-processing the outcome of true annealing with iterative improvement was found to produce satisfactory results.

Stopping Criterion

In most applications of annealing, a very low value of normalized objective function is used as the stopping criterion. The use of a very low value implies a high degree of confidence in the value of the idealized or training measures embedded in the objective function. But in earth

science applications, our information from the subsurface and even outcrop is often incomplete and matching the Markov transition frequencies exactly may not be warranted. As mentioned in the introduction, a chi-squared test statistic can be used determine if an observed Markov chain or its embedded form are significantly different from a random series of events. The same formulation can be used to determine if two Markov transition matrices are different from each other at some level of statistical significance (Powers and Easterling, 1982). Table 3 compares the values of the normalized objective function and associated numbers of perturbations needed to anneal a single isotropic field with the structure of Table 1C with different stopping criteria based on the chi-squared test statistic. One can see that, as the level of statistical significance employed in the chi-squared test decreases from 0.20 to 0.01, it becomes increasingly easy to accept that the annealed field is not significantly different from the training structure with commensurate computational savings in the form of fewer perturbations. Figure 4 shows the same stopping points on a plot of the objective function trajectory. Because iterative improvement was used in this relatively simple example, the objective function trajectory is quite steep and the computational savings associated with using a chi-squared test as a stopping criterion are not profound. However, when the objective function becomes less steep, the computational savings associated with reaching a normalized objective function value in the order of $1x10^{-3}$ or $1x10^{-4}$ can be substantial compared to the effort needed to reach a value in the order of $1x10^{-6}$.

Effects of Conditioning

Stochastic images generated by annealing can be constrained or "conditioned" to honor field observations simply by assigning the appropriate grid locations the observed values and not perturbing them. This approach produces undesirable discontinuities in the vicinity of the conditioning data. The discontinuities can be smoothed by weighting the contribution of any part of the global objective function involving conditioning data heavier than non-conditioning grid blocks (Deutsch and Cockerham, 1994). Figure 5 shows an experiment wherein a 100x100 field with the structure in Table 1C was conditioned to match data from a vertical "well" of lengths 5, 25, and 100 blocks. The values of the well data were obtained by sampling a different unconditional realization with the same structure. In this case, a weighting of 5 was used on

transition probabilites that involved conditioning data. For the cases of wells of lengths 5 and 25 grid blocks, true annealing reached a satisfactory threshold of the normalized objective function based on a chi-squared test statistic at a 0.01 level of significance. The detail of the well around the 25-block well shows that the field has been acceptably smoothed. We found that weights higher than 5 degraded the annealing performance rapidly. The objective function trajectory for the field conditioned by a 100-block well became trapped in an unacceptable local minimum before passing the chi-squared threshold.

CAPTURING GEOLOGICALLY MEANINGFUL STRUCTURES IN STOCHASTIC FIELDS WITH MARKOV STRUCTURES

The previous section demonstrated that embuing stochastic fields with Markov properties is reasonably straightforward using simulated annealing provided that attention is paid to some key performance issues. In this section we look at some examples of styles of stratal architecture that can be embedded in stochastic fields by this approach. The first examples shown are hypothetical but we trust they demonstrate some of the potential of applying this technique to simulation of real rock systems. In the final example, an unconditioned stochastic image of the Gloucester confining layer is presented to demonstrate that these ideas can be carried out with field data.

Example 1: First versus Second-Order Structure

As discussed above, Markov chains and fields can possess a higher than single order structure. Table 4 shows a hypothetical, three-state structure. The structure is shown in the form of three transition probability matrices. Matrix 4A shows the transition probability structure going from location $x+1$ from x given that the Markov chain is in state "Black" at locaton $x-\tau$ where we have arbritrarily chosen $\tau=9$ grid units. Likewise, Matrix 4B shows transition matrices if the Markov chain is in state "Gray" at $x-\tau$ and 4C shows the probabilities is the Markov chain is in state "White" at $x-\tau$. Higher order structures are discussed in detail in Harbaugh and Bonham-Carter (1970). Table 4D shows the first-order Markov structure "embedded" in the second-order structure of Table 4A-4C. Two 100x100 fields were generated by annealing using multipoint

histograms to enforce the second-order structure as well as the first-order structure of Table 4. These two fields are shown as gray-scale images in Figure 6. Accompanying the fields are indicator variograms for each of the three categorical states. From the gray-scale images, it appears that the second-order Markov image has more structure than the first-order image. The second-order image appears to have move extensive areas of predominantly gray or white pixels. The gray and white categories show strong-reduction in indicator semivariance at the lag corresponding to the spatial wavelength of the second-order structure. These structures in the indicator variograms are a measure of the statistical structure in the second-order Markov image that is lacking in the first-order Markov image.

Example 2: Directionality and Cyclicity

The concepts of directionality and cyclicity in Markov Chains were introduced above. Directionality is common in many sedimentary depositional environments, e.g., consider shoaling-upward sequences on carbonate banks or fining-upward sequences in channel deposits. Directionality means there will be an up and down, or a basinward-and landward asymmetry in a bedding sequence. Cyclicity or the regular, non-random repetition of beds is also common in the rock record. In Markov chains, cyclicity is detected by the presence of complex eigenvalues in the transition probabiliy matrix (Schwarzacher, 1975). The hypothetical transition probability matrix in Table 5A has obvious cyclicity and has complex eigenvalues as shown. Directionality is also evident in the embedded form - there is a distinct directionality in the off-diagonal elements that would change if the chain was run backwards. A single two-dimensional field with this transition matrix enforced in the vertical and horizontal directions is shown as a grayscale image in Figure 7A.

For comparison, the directionality and cyclicity was removed in the horizontal direction by averaging the off-diagonal elements in the Markov structure as shown in Table 5B. Note that the complex eigenvalues have now disappeared. The symmetric structure of Table 5B was enforced in the horizontal in the grayscale image in Figure 7B, leaving the vertical structure as before. This example highlights the flexibity of annealing to capture hybrid structures that better accommodate

geological concepts of reasonableness. There are many geological environments where directionality and cyclicity are apparent in vertical bedding relationships but does not extend to realtionships in the horizontal.

Example 3: Honoring Time-Spatial Relationships in Markov Representations of Strata: Going from the Vertical to the Horizontal with Walther's Law

Doveton (1994) revisits the common suggestion that Markov measures of vertical variability from boreholes may be transferred to the horizontal to inform a description of horizontal variability. If Markov structures are to have a use in injecting geologic realism into stochastic models, then this suggestion warrants further examination.

The geological justification for this transference comes through invocation of Walther's Law of Facies Succession, an operating principle of stratigraphy. According to Middleton's translation (1973), Walther's Law was originally stated as follows:

> 'The various deposits of the same facies areas and similarly the sum of the rocks of different facies areas are formed beside each other in space, though in cross-section we see them lying on top of each other. As with biotopes, it is a a basic statement of far-reaching significance that only those facies and facies areas can be superimposed primarily which can be observed beside each other at the present time."

Middleton emphasizes: " Walther's Law leads us to expect that each facies will show only certain transitions to other facies, but it does not suggest that all of the genetically related facies can be arranged in a single sequence, because some facies may represent alternatives at a given stage in the development of any particular cycle".

This statement gives the justification for using Walther's Law for translating vertical Markov measures of variability to the horizontal in a probabilistic framework. Recast in Markovian terms, one might restate Walther's Law as follows: If the probability of any state succeeding another in

the vertical is equal to the probability that the states developed adjacently at a given time, then the probabilities of any state being juxtaposed horizontally should equal the probability that states are vertically superimposed, provided the horizontal juxtaposition is coeval. The probabilistic approach can also accommodate minor erosional breaks in a succession as a component of random noise (Doveton, 1994). This assumption will only work so long as the depositional process is stationary at the scale of interest.

If Walther's Law of facies succession is used to justify transfer of Markov measures of vertical variability in bedding sequences to the horizontal, a coordinate transformation from vertical space to vertical time must considered that ensures that horizontal surfaces equal time lines. The coordinate transformation necessary to transfer vertical Markov measures to the horizontal along time lines is a simple rescaling of each category separately according to their relative depositional rates. The mechanics of this rescaling (Schwarzacher, 1969) is shown in Figure 8A, where a hypothetical three-lithology system is rescaled from transitions counted in space to equivalent transitions in time assuming that the relative depositional rates of sandstone, shale, and limestone are 1.0, 0.5, and 0.33, respectively. This rescaled Markov temporal structure was enforced in the vertical direction of a 100x100 field in Figure 8B whereas the horizontal structure enforced was the original Markov spatial structure. This realization was backtransformed to vertical spatial coordinates by post-processing in such a way as to compress the limestone and shale pixels vertically in inverse proportion to their relative rates of deposition. Markov fields constructed in a Waltherian framework should conserve the sediment, time, and volume elements of a depositional system. Prior to vertical back-transformation, Markov fields could be regarded as synthetic Wheeler diagrams (Wheeler, 1958).

If desired, compaction effects can be similarly incorporated. Similarly, significant gaps in the sedimentary record due to erosion and nondeposition are accounted for as a nondepositional or erosive state existing through time. It is conceivable that if sufficient geochronological or biostratigraphic data exist to reconstruct these states, they could enter a Markov model as a category in a mixed coordinate system that is removed in the backtransformation.

Example 4: A Stochastic Image of the Gloucester Site Confining Layer.

Figure 9 shows the final example: a 100x100 2D stochastic image of the confining layer at the Gloucester site. All of the structures encapsulated in the Markov transition matrix in Table 2 are present in this image. The effort required to anneal this image was shown above in Figure 3. Annealing this image was difficult, but not impossible, because of the number of states present, the low ratio of grid size to mean body lengths, and the complexity of the structure. This example demonstrates that field data can be gathered from borehole cores, translated into a meaningful Markov probability structure and used to inform a stochastic image of a complex geological system by annealing in a form completely suitable for use in flow simulation.

SUMMARY

In this paper, we demonstrate how conditioned structured fields honouring Markov transition probability structures can be generated with simulated annealing. To guide future applications of this technique, the performance issues pertaining to scale effects, structural complexities, and choice of stopping criteria were discussed and remedies offered, namely:

- Scale Effects. As categorical length scales increase relative to grid size, annealing performance diminishes. The general remedy is to use a larger grid.
- Complexity Effects. As number of states, variation in categorical length scales, or complexity in the embedded Markov chain increase, annealing performance diminishes. The remedy is to choose a larger grid or possibly try a combination of annealing routines.
- Stopping Criteria. To remedy complexity effects or to reduce computational cost, a chi-squared test statistic can be used to evaluate if the annealed image is significantly different than the training image at some predetermined level of confidence. This approach can be justified when the Markov model is being estimated from incomplete subsurface data or is otherwise incompletely known. Incorporation of such a stopping criterion may be also considered when Markov structures are to be blended with other kinds of structures in an objective function.

By incorporating Markov structures in stochastic simulation of real rock systems, one can capture more geologic realism. We show how Markov structures can capture geological complexities in natural systems pertaining not only to length scales and categorical interrelationships but also stratal achitecture pertaining to aspects of depositional process: higher -order structures, cyclicity, and directionality. The flexibility of this approach to accomodate geological reasoning through hybrid structures and rescaling to honor time-space relationships in real rock systems was highlighted. An example is shown where field data taken from borehole cores was successfully transmitted to a stochastic image by this method.

Acknowledgements

This work has been supported through the Amoco Canada Petroleum Company Ltd. Graduate Fellowship in Geology at the University of Calgary. Additional support has been provided by the Environment Canada through the National Water Research Institute, Canada Centre for Inland Waters, the Canada NSERC Grant No. OGP0122023, and the Department of Geology and Geophysics, University of Calgary.

REFERENCES

Carle, S.F, and G.E. Fogg, 1996. Transition probability-based indicator geostatistics. Mathematical Geology, vol. 28, no. 4, p. 453-478.

Davis, J.C., 1986. Statistics and Data Analysis in Geology. 2nd Edition. J.Wiley & Sons, New York, 646 pp.

Deutsch, C.V. and P.W. Cockerham, 1994. Practical considerations in the application of simulated annealing to stochastic simulation. Mathematical Geology, vol. 26, no. 1, p. 67-82.

Deutsch, C.V., and T.A. Hewitt, 1996. Challenges in reservoir forecasting. Mathematical Geology, vol. 28, no. 7, p. 829-842.

Deutsch C.V. and A.G. Journel, 1992. GSLIB Geostatistical Software Library and User's Guide. Oxford University Press, New York. 340 pp.

Doveton, J.H., 1994. Theory and Application of Vertical Variability Measures from Markov Chain Analysis. In: Yarus, J.M., and R.L. Chambers, eds., Stochastic Modeling and Geostatistics - Principles, Methods and Case Studies. AAPG Computer Applications in Geology, No. 3. American Association of Petroleum Geologists, Tulsa, Oklahoma. p. 55-64.

Farmer, C.L., 1992. Numerical Rocks. In King, P.R., ed., Proceedings of the First European Conference on The Mathematics of Oil Recovery, 1989. Oxford University Press, p. 437-448.

Gailey, R.M., and S.M. Gorelick, 1993. Design of optimal, reliable plume capture schemes: application to the Gloucester Landfill ground-water contamination problem. Ground Water, vol. 31, no. 1, p. 107-114.

Harbaugh, J.W., and G. Bonham-Carter, 1970. Computer Simulation in Geology. John Wiley & Sons, Toronto, 575 pp.

Jackson, R.E., S. Lesage, M.W. Priddle, A.S. Crowe, and S. Shikaze, 1991. Contaminant Hydrogeology of Toxic Organic Chemicals at a Disposal Site, Gloucester, Ontario. 2. Remedial Investigation. Inland Waters Directorate Scientific Series No. 181. National Water Research Institute, Environment Canada, Burlington, Ontario. 68 pp.

Jensen, J.L., L.W. Lake, P.W.M. Corbett, and D.J. Goggin, 1997. Statistics for Petroleum Engineers and Geoscientists. Prentice Hall, N.J., 390 pp.

Koltermann, C.E., and S.M. Gorelick, 1996. Heterogeneity in sedimentary deposits: A review of structure-imitating, process-imitating, and descriptive approaches. Water Resources Research, vol. 32, no. 9, p. 2617-2658.

Krumbein, W.C., 1967. Fortran IV Computer Programs for Markov Chain Experiments in Geology. Kansas State Geological Survey Computer Contribution 13.

Lin, C. and Harbaugh, J.W., 1984. Graphic Display of Two- and Three-Dimensional Markov Computer Models in Geology. Van Nostrand Reinhold, New York.

Luo, J., 1996. Transition probability approach to statistical analysis of spatial qualitative variables in geology. *In*: Forster,A., and D.F. Merriam, eds., Geologic Modeling and Mapping. Plenum Press, New York. p.281-297.

Middleton, G.V., 1973. Johannes Walther's Law of the Correlation of Facies. Geological Society of America Bulletin, vol. 84, p. 979-988.

Moss, B.P., 1990. Stochastic reservoir description: a methodology. In: Morton, A.C., A. Hurst, and M.A. Lovell, eds., Geological Applications of Wireline Logs. Geological Society Special Publication No. 48, p. 57-76.

Murray, C.J., 1994. Identification and 3-D Modeling of Petrophysical Rock Types. In: Yarus, J.M., and R.L. Chambers, eds., Stochastic Modelling and Geostatistics - Principles, Methods, and Case Studies. AAPG Computer Applications in Geology, No. 3, p. 55-64.

Ouenes, A., and S. Bhagavan, 1994. Application of simulated annealing and other global optimization methods to reservoir description: myths and realities. Society of Petroleum Engineers Paper 28415.

Parks, K., 1998. Geosystem Modeling with Markov Chains and Simulated Anneling. Unpublished Ph.D. Dissertation, University of Calgary, 296 pp.

Powers, D.W., and R.G. Easterling, 1982. Improved methodology for using embedded Markov chains to describe cyclical sediments. Journal of Sedimentary Petrology, vol. 52, no. 3, p. 913-923.

Schwarzacher, W., 1969. The use of Markov chains in the study of sedimentary cycles. Mathematical Geology vol. 1, no. 1, p 17-39.

Schwarzacher, W., 1975. Sedimentation Models and Quantitative Stratigraphy. Developments in Sedimentology 19, Elsevier, 382 pp.

Walker, R.G., 1979. Facies and Facies Model. General Introduction. In: R.G. Walker, ed. Facies Models, 1st Edition. Geoscience Canada Reprints Series 1. p. 1-8.

Wheeler, H.A., 1958. Time stratigraphy. AAPG Bulletin, vol. 42, no. 5, p. 1047-1063.

Xu, H., and A.J. MacCarthy, 1996. Markov chain analysis of vertical facies sequences using a computer softward package (SAVFS): Courtmacsherry Formation (Tournaisian), Southern Ireland. Computers & Geosciences Vol, 24, no. 2, p. 131-140.

LIST OF TABLES

LIST OF FIGURES

Figure 1. Objective function trajectories for four 3-state Markov structures with no embedded structures and different categorical length scales.. In 1A, P_{ii}=0.60 for each state; in 1B, 0.70; in 1C, 0.80; in 1D, 0.90. The corresponding mean body lengths for each P_{ii} (Eqn. 4) are 1A: 1.5, 1B: 2.3, 1C: 4.0, and 1D:9.0 units. The grid size is 100x100 units. The ratios of grid size to mean body lengths are 66.7, 42.9, 25.0, and 11.1 units, respectively. As this ratio decreases, annealing performance dimishes.

Figure 2: Objective function trajectories (using iterative improvement) for four, 3-state Markov structures (A-D) with increasingly complicated structures corresponding to those shown in Table 1A-1D. The trajectory E is that for the 5-state structure for the Gloucester confining layer in Table 2. All trajectories come from a single annealing run. Comparison of the trajectories shows that, in general, as complexity of Markov structure increases, the angle of descent of the annealing trajectory tends to decrease.

Figure 3: Objective function trajectories for the 5-state Markov structure in Table 2 comparing the annealing performance of iterative improvement (Trajectory A) to that of true annealing post-processed with iterative improvement (Trajectory B). The combined approach succeeded in reducing the objective function value to an acceptable minimum whereas the iterative improvement approach became trapped in an unacceptable minimum. The performance of true annealing alone (first segment of Trajectory B) also was unsuccessful in reducing the objective function to an acceptable minimum within a tolerable number of perturbations.

Figure 4: Stopping points from Table 3 placed on the objective function trajectory (iterative improvement used).

Figure 5: Effect of conditioning on annealing performance. Trajectories on left show annealing performance when a 100x100 3-state field is conditioned to honor a vertical well of length A) 5 units, B) 25 units, and C) 100 units. True annealing was used. Stopping criterion is when the

calculated chi-squared test statistic fell below13.2, corresponding to a level of significance of 0.01 and 5 degrees of freedom. Run C became trapped in a local minimum before satisfying the stopping criterion. The weighting on the conditioning pairs was set to 5.0. The field on the right shows detail of field B in the vicinity of the conditioning well (outline). The underlying Markov structure is that in Table 1C.

Figure 6. Comparison of first and second-order, 3-state Markov fields as shown in Table 4. Comparative indicator variograms (I(h)) are shown for each state. The gray and white states show a strong reduction in indicator semivariance at the lag corresponding to the spatial wavelength of the second-order structure.

Figure 7. Comparison of detail from two 100x100 unit fields honoring the first-order, 3-state Markov structures in Table 5. In field A, the directionality and cyclity of Table 5A is enforced in both the vertical and the horizontal. Field B is a hybrid field, combing the structure of Table 5A in the vertical and that of 5B (no directionality or cyclity) in the horizontal.

Figure 8. Illustration of conversion of a 3-state Markov field from spatial coordinates to equivalent temporal coordinates and back using relative rates of depostion to rescale vertical categorical length scales. The top field is generated in mixed time-space coordinates with time in the vertical. The bottom field is the same but back-transformed to pure spatial coordinates. Black represents unfilled space.

Figure 9: Unconditional panel reproduction of the Gloucester confining layer generated from field-data derived, 5-state, first-order Markov structure shown in Table 2. The field was generated by the combined approach shown in Figure 3.

TABLE 1

P(J)|I	B	G	W
B	0.60	0.20	0.20
G	0.20	0.60	0.20
W	0.20	0.20	0.60

Full Transition Matrix

P(J)|I	B	G	W
B	0.00	0.50	0.50
G	0.50	0.00	0.50
W	0.50	0.50	0.00

Embedded Matrix

A. 3 states, all same length scale, no embedded structure

P(J)|I	B	G	W
B	0.60	0.30	0.10
G	0.10	0.60	0.30
W	0.30	0.10	0.60

Full Transition Matrix

P(J)|I	B	G	W
B	0.00	0.75	0.25
G	0.25	0.00	0.75
W	0.75	0.25	0.00

Embedded Matrix

B. 3 states, all same length scale, embedded structure with preferred cyclicty of B-G-W-B-G-W...

P(J)|I	B	G	W
B	0.60	0.30	0.10
G	0.075	0.70	0.225
W	0.15	0.05	0.80

Full Transition Matrix

P(J)|I	B	G	W
B	0.00	0.75	0.25
G	0.25	0.00	0.75
W	0.75	0.25	0.00

Embedded Matrix

C. 3 states with different length scales but same embedded structure as B.

P(J)|I	B	G	W
B	0.60	0.30	0.10
G	0.10	0.70	0.20
W	0.10	0.10	0.80

Full Transition Matrix

P(J)|I	B	G	W
B	0.00	0.75	0.25
G	0.67	0.00	0.33
W	0.50	0.50	0.00

Embedded Matrix

D. 3 states with same length scales as C but more complex embedded structure.

TABLE 2

P(J)|I	Med. Sand	Fine Sand	Silt	Clay	Diamict
Med. Sand	0.8965	0.0460	0.0345	0.0115	0.0115
Fine Sand	0.0048	0.8350	0.0271	0.1133	0.0197
Silt	0.0290	0.0580	0.7971	0.1014	0.0145
Clay	0.0013	0.0583	0.0265	0.9007	0.0132
Diamict	0.0253	0.0633	0.0000	0.0506	0.8608

5-state lithofacies transition matrix associated with aquitard bedding derived from vertical core data from Gloucester Landfill site, Ontario,

P(J)|I	Med. Sand	Fine Sand	Silt	Clay	Diamict
Med. Sand	0.0000	0.4444	0.3333	0.1111	0.1111
Fine Sand	0.0297	0.0000	0.1642	0.6867	0.1194
Silt	0.1429	0.2859	0.0000	0.4998	0.0715
Clay	0.0131	0.5871	0.2669	0.0000	0.1329
Diamict	0.1818	0.4547	0.0000	0.3635	0.0000

5-state embedded transition matrix associated with aquitard bedding in cores from the Gloucester Landfill site, Ontario, Canada.

TABLE 3

Stopping Critera	Normalized Objective Function	Number of Perturbations
Objective Function < 1e-6 (χ^2_{obs} = 0.641e-01)	0.650e-06	96589
$\chi^2_{obs}<\chi^2_{\alpha,\nu}$ = 5.99: α = 0.20, ν = 4	0.830e-04	88663
$\chi^2_{obs}<\chi^2_{\alpha,\nu}$ = 7.78: α = 0.10, ν = 4	0.108e-03	87639
$\chi^2_{obs}<\chi^2_{\alpha,\nu}$ = 9.49: α = 0.05, ν = 4	0.132e-03	86809
$\chi^2_{obs}<\chi^2_{\alpha,\nu}$ = 11.14: α = 0.025, ν = 4	0.154e-03	86233
$\chi^2_{obs}<\chi^2_{\alpha,\nu}$ = 13.28: α = 0.01, ν = 4	0.188e-03	85455

α = level of significance μ = degrees of freedom

TABLE 4

	B	G	W
B	0.85	0.075	0.075
G	0.075	0.85	0.075
W	0.075	0.075	0.85

A. P(K)|J|I=B)

	B	G	W
B	0.65	0.175	0.175
G	0.20	0.55	0.25
W	0.20	0.55	0.25

B. P(K)|J|I=G)

	B	G	W
B	0.60	0.20	0.20
G	0.35	0.25	0.40
W	0.25	0.25	0.50

C. P(K)|J|I=W)

	B	G	W
B	0.80	0.10	0.10
G	0.21	0.50	0.29
W	0.23	0.25	0.52

D. P(J)|I

TABLE 5

P(J)|I	B	G	W
B	0.60	0.37	0.03
G	0.03	0.60	0.37
W	0.37	0.03	0.60

Eigenvalues: 1.00, 0.4+.294i, 0.4-.294i

A

P(J)|I	B	G	W
B	0.60	0.20	0.20
G	0.20	0.60	0.20
W	0.20	0.20	0.60

Eigenvalues: 1.00, 0.40, 0.40

B

FIGURE 1

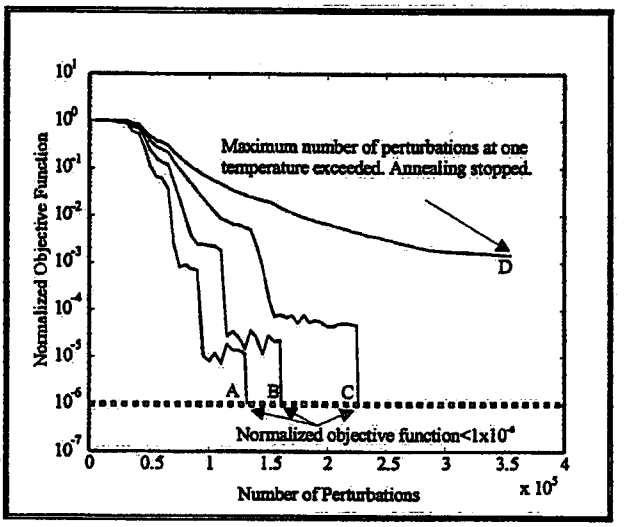
Normalized Objective Function
Maximum number of perturbations at one temperature exceeded. Annealing stopped.
D
A
B
C
Normalized objective function<1x10⁻⁶
Number of Perturbations
x 10⁵

FIGURE 2

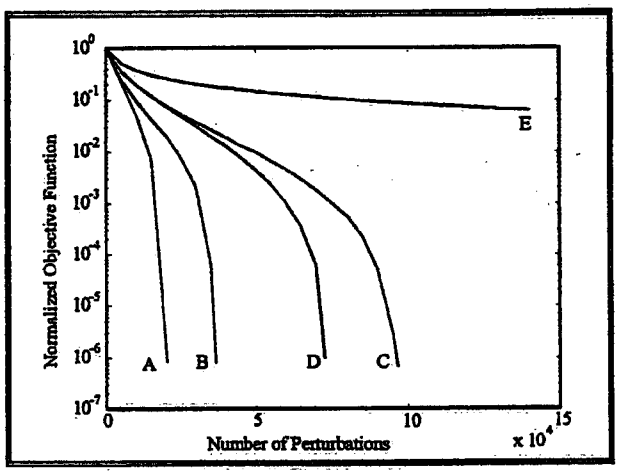
Normalized Objective Function
10^{0}
10^{-1}
10^{-2}
10^{-3}
10^{-4}
10^{-5}
10^{-6}
10^{-7}
A
B
D
C
E
0
5
10
15
Number of Perturbations
x 10^{4}

FIGURE 3

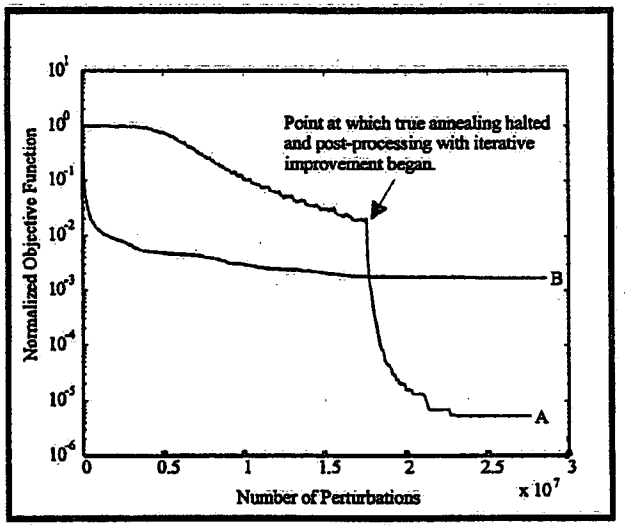
Normalized Objective Function
10^{1}
10^{0}
10^{-1}
10^{-2}
10^{-3}
10^{-4}
10^{-5}
10^{-6}
Point at which true annealing halted and post-processing with iterative improvement began.
B
A
0
0.5
1
1.5
2
2.5
3
Number of Perturbations
x 10^{7}

FIGURE 4

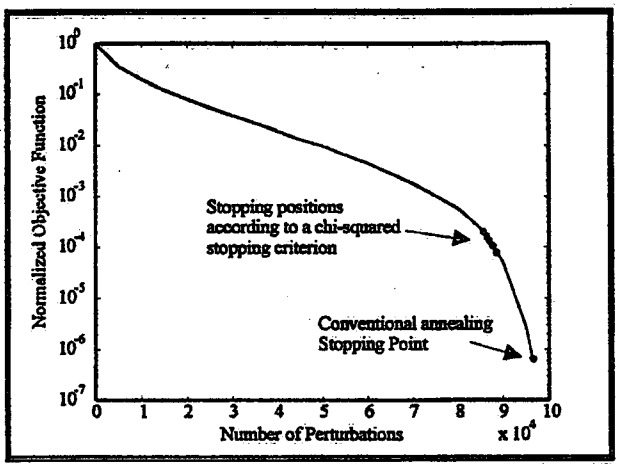
Normalized Objective Function
10^{0}
10^{-1}
10^{-2}
10^{-3}
10^{-4}
10^{-5}
10^{-6}
10^{-7}
Stopping positions
according to a chi-squared
stopping criterion
Conventional annealing
Stopping Point
0 1 2 3 4 5 6 7 8 9 10
Number of Perturbations
x 10^{4}

FIGURE 5

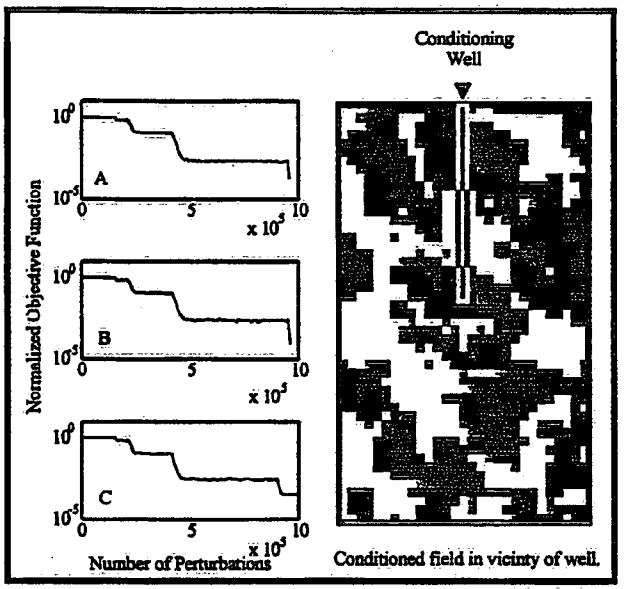
Conditioning
Well
Normalized Objective Function
A
B
C
10^0
10^{-5}
0
5
10
x 10^5
Number of Perturbations
Conditioned field in vicinity of well.

FIGURE 6

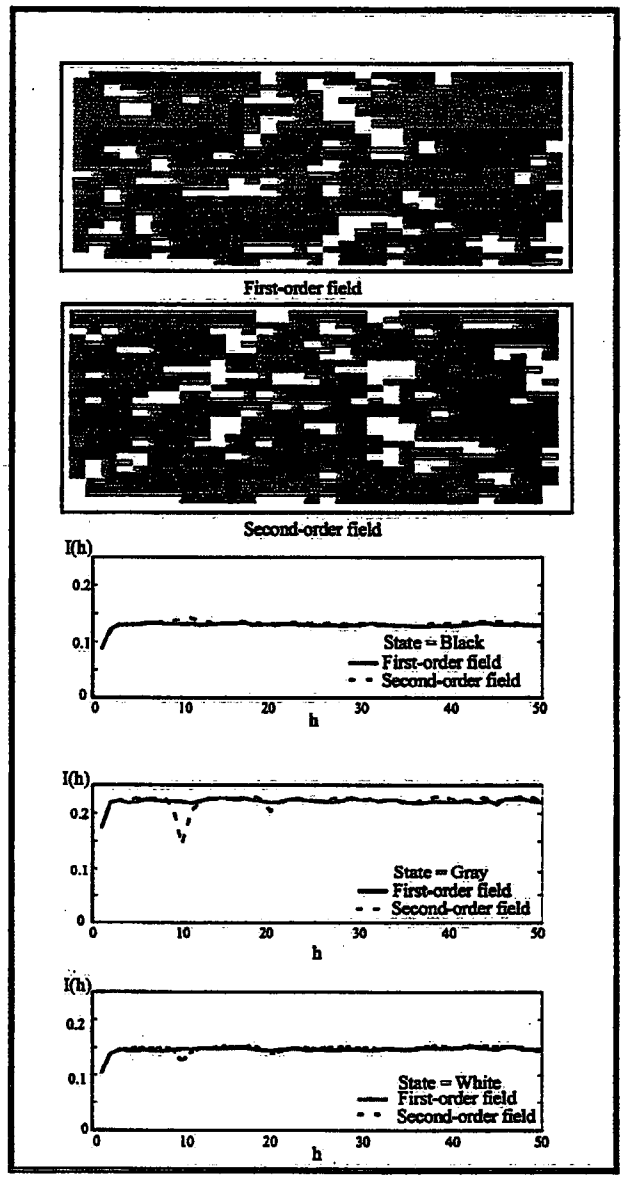
First-order field
Second-order field
I(h)
0.2
0.1
0
State = Black
First-order field
Second-order field
0
10
20
30
40
50
h
I(h)
0.2
0.1
0
State = Gray
First-order field
Second-order field
0
10
20
30
40
50
h
I(h)
0.2
0.1
0
State = White
First-order field
Second-order field
0
10
20
30
40
50
h

FIGURE 7

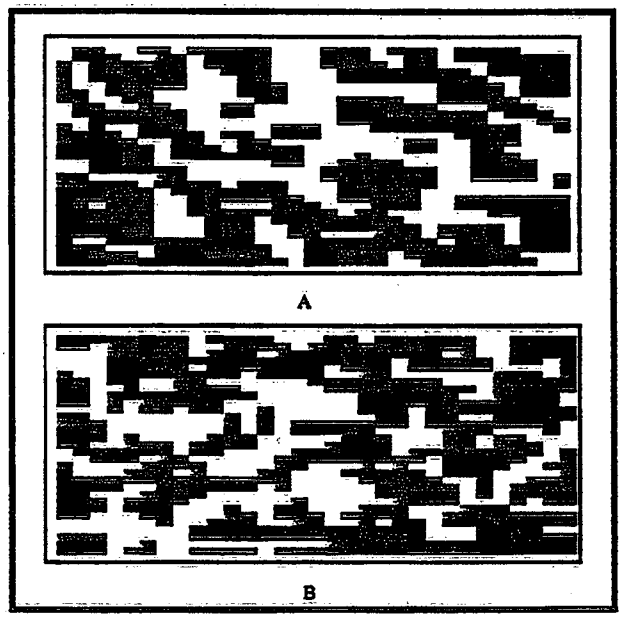

FIGURE 8

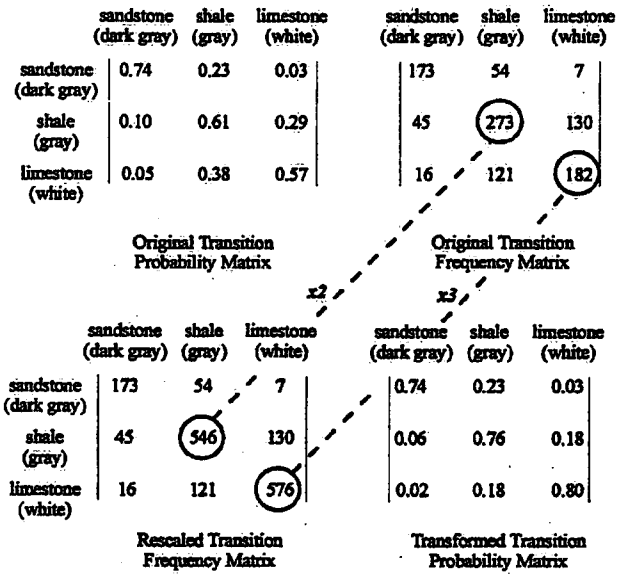
sandstone (dark gray)
shale (gray)
limestone (white)
sandstone (dark gray) 0.74 0.23 0.03
shale (gray) 0.10 0.61 0.29
limestone (white) 0.05 0.38 0.57
Original Transition Probability Matrix
sandstone (dark gray) 173 54 7
shale (gray) 45 273 130
limestone (white) 16 121 182
Original Transition Frequency Matrix
x2
x3
sandstone (dark gray) 173 54 7
shale (gray) 45 546 130
limestone (white) 16 121 576
Rescaled Transition Frequency Matrix
sandstone (dark gray) 0.74 0.23 0.03
shale (gray) 0.06 0.76 0.18
limestone (white) 0.02 0.18 0.80
Transformed Transition Probability Matrix

FIGURE 9

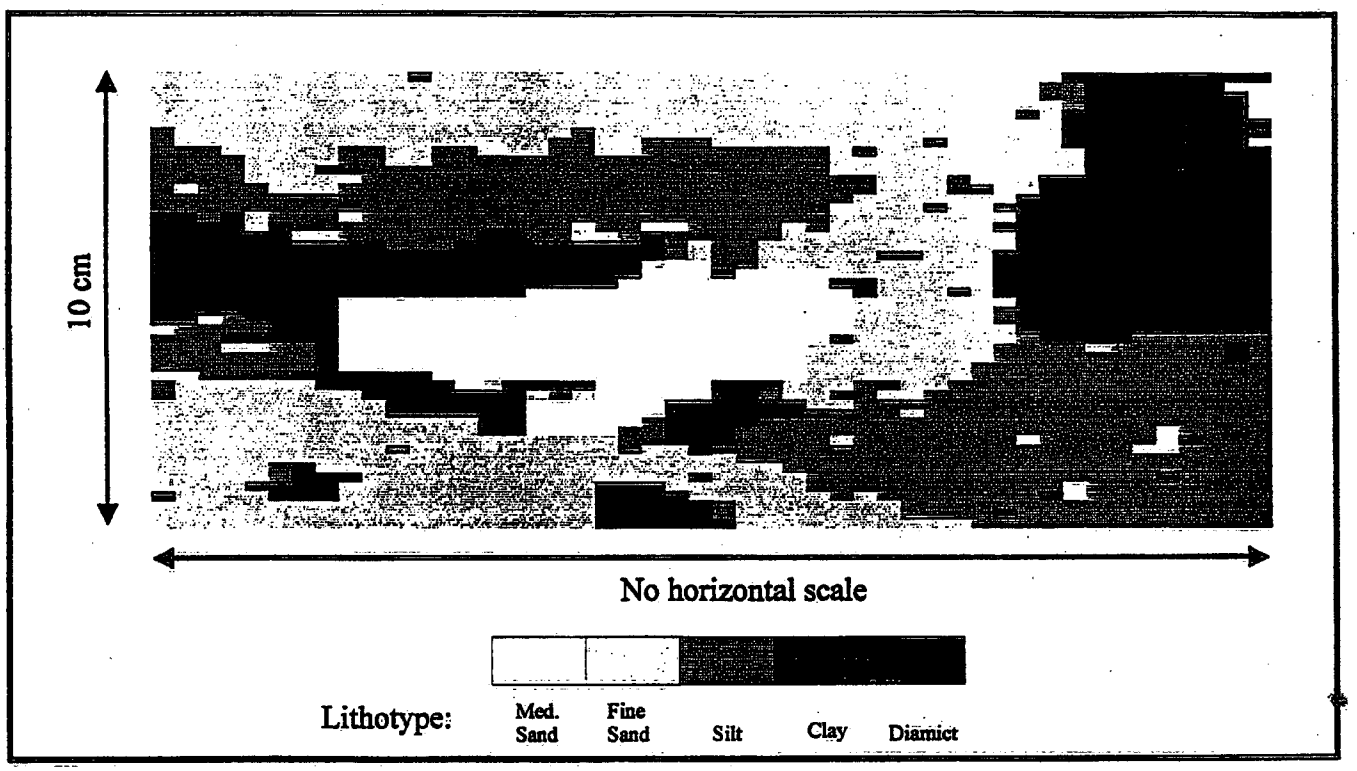
10 cm
No horizontal scale
Lithotype:
Med. Sand
Fine Sand
Silt
Clay
Diamict

PRINTED IN CANADA
IMPRIMÉ AU CANADA
ON RECYCLED PAPER
SUR DU PAPIER RECYCLÉ

National Water Research Institute
Environment Canada
Canada Centre for Inland Waters
P.O. Box 5050
867 Lakeshore Road
Burlington, Ontario
L7R 4A6 Canada

National Hydrology Research Centre
11 Innovation Boulevard
Saskatoon, Saskatchewan
S7N 3H5 Canada

NATIONAL WATER RESEARCH INSTITUTE
INSTITUT NATIONAL DE RECHERCHE SUR LES EAUX

Institut national de recherche sur les eaux
Environnement Canada
Centre canadien des eaux intérieures
Case postale 5050
867, chemin Lakeshore
Burlington, Ontario
L7R 4A6 Canada

Centre national de recherche en hydrologie
11, boul. Innovation
Saskatoon, Saskatchewan
S7N 3H5 Canada

Canada

Environment Canada Environnement Canada